

Mathematical analysis of a flux-jump model in superconductivity

Jean-Guy Caputo and Nathan Rouxelin¹

¹*INSA Rouen Normandie, LMI UR 3226, F-76000 Rouen,
France E-mail: jean-guy.caputo@insa-rouen.fr, nathan.rouxelin@insa-rouen.fr*

We analyzed mathematically a model describing flux jumps in superconductivity in a 1D configuration. Three effects occur from fastest to slowest: Joule heating, magnetic relaxation and temperature diffusion. Adimensionalising the equations showed that magnetic field fronts penetrate the material as inhomogeneous Burgers fronts. An additional global term pushes the magnetic field and is responsible for flux jumps. We considered a medium temperature for which the heat capacity of a sample can be taken as a constant and a low temperature where heat capacity depends on temperature causing a nonlinear temperature evolution. As expected, we found that flux jumps occur mostly at low temperature. To understand flux trapping, we examined external magnetic field pulses of different amplitudes and duration. We found that flux trapping is maximal for medium amplitudes and low temperatures.

PACS numbers:

Keywords

Type II superconductor, flux jump, Burger's equation

References

10

Contents

I. Introduction	1
II. Physical model	2
A. Simplified 1D configuration	2
B. Time scales	3
C. Normalization	4
1. High temperature: C constant	4
2. Low temperature: $C(T)$	5
3. Boundary conditions	5
III. Numerical method	5
A. Magnetic field pulse	6
IV. Numerical results for constant C	6
A. Influence of B_e for $T_e = 0.5$	6
B. Magnetization	7
C. Pulse duration	7
V. Numerical results for $C(T)$	8
A. Influence of B_e for $T_e = 0.1$	8
B. Flux jump in magnetization : optimal B_e and pulse duration	9
VI. Conclusion	10

VII. Appendix: fixed point of the equations and oscillation

I. INTRODUCTION

High T_c superconductivity has seen the advent of strong and flexible superconducting magnets that can be used for screening magnetic fields in medical instruments and to build ultra light motors for transportation and power, see the roadmap by Durrell et al [1] for all the possible applications. The main technique to make a magnet is to submit a cooled sample to a strong magnetic pulse: Pulse Field Magnetization [1]. During the process, a flux jump i.e. a sudden change of the total magnetization of the sample due to heating can occur and change the properties of the magnet, see the experiments [2], [5], [3] done with MgB_2 and $YBaCuO$ materials.

A microscopic explanation of these flux jumps based on the Ginzburg-Landau free energy involves a complex interaction inside the sample of the network of vortices with the network of defects that usually trap them; this is analyzed very clearly by Campbell and Evetts [6]. Even in 1D, coupling Maxwell's equations with the Ginzburg-Landau equations for the order parameter to understand how vortices are induced and interact in a material is challenging [4]. Temperature effects are ignored and they are important because they change the parameters and allow vortex motion. The final issue is that samples have a size of the order of the cm while the size of a vortex is about $1 \mu m$ so that there are about 10^4 vortices in a typical sample. For all these reasons one should consider a macroscopic model, the critical state model together with an equation for the temperature.

The critical state model is a phenomenological con-

stitutive equation $E(J)$ connecting the electric field E to the current density J . This gives rise to a nonlinear diffusion equation for the magnetic field B coupled to an inhomogeneous diffusion equation for the temperature T . Also note that flux jumps are a dynamical effect and depend on how the external magnetic field B_e is applied, therefore one needs to specify the external field dynamics. In addition, many of the flux jumps described in the literature occur in complicated 2D or even 3D experimental setups. The modeling is done using a finite element software and few details are given about the numerical procedure. In particular, it is hard to understand the mechanisms of these flux jumps. To clarify these issues, important questions are

- what are the time scales of the different phenomena involved in the process?
- what physical conditions lead to flux jumps?
- do flux jumps occur at specific values of the field?
- what is the external field dynamics that gives a maximal field trapping?

To answer these questions we considered a 1D situation where the geometry of the fields is not complicated and a standard constitutive equation. We wrote the equations in dimensionless form identifying the typical time scales. Using this model, we examined the influence of the different parameters in particular the heat capacity. We varied systematically the pulse magnitude and duration to see how they influence the trapped field and the flux jumps. We were able to understand the mechanism of flux jumps by detailing the terms in the evolution of B . In addition, we analyzed the trapped flux as a function of the pulse duration.

The article is organized as follows: section 2 presents the physical configuration and model and its dimensionless form. Section 3 describes the time dynamics of the magnetic pulse together with the numerical method used to solve. Sections 4 and 5 give the results for medium and low temperatures respectively and section 6 concludes the article.

II. PHYSICAL MODEL

The magnetic behavior of a type II superconductor is given by the Maxwell equations and a constitutive law. The Maxwell equations read

$$\nabla \times \mathbf{E} = -\partial_t \mathbf{B}, \quad (1)$$

$$\nabla \times \mathbf{B} = \mu_0 \mathbf{J}, \quad (2)$$

where \mathbf{E} , \mathbf{B} are the electric and magnetic fields, \mathbf{J} is the current density and the term $\partial_t \mathbf{E}$ is neglected (quasi-static regime). The constitutive law is

$$\mathbf{E} = \mathbf{E}(\mathbf{J}), \quad (3)$$

where \mathbf{E} and \mathbf{J} are parallel. The evolution of the temperature of the sample is given by

$$\rho_d C \partial_t T = \mathbf{E} \cdot \mathbf{J} + \kappa \Delta T, \quad (4)$$

where $\mathbf{E} \cdot \mathbf{J}$ is the power heating per unit volume due to the magnetic field.

A. Simplified 1D configuration

To understand in detail the interplay between the magnetic field and the temperature, we follow the authors of [2] and reduce the problem to one dimension.

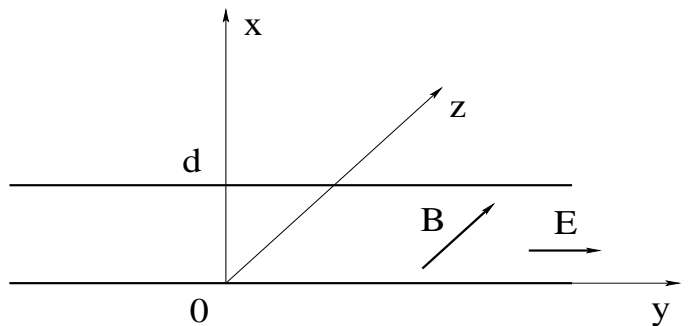


FIG. 1: Simplified configuration: infinite superconducting plate of thickness $2d$.

We consider a superconducting plate of thickness $d \gg \lambda$, infinite along y and z , see Fig. 1. An external time dependent magnetic field $\mathbf{B}_e(t)$ is applied along z . Then we can write

$$\mathbf{B} = (0, 0, B(x, t))^T, \quad \mathbf{E} = (0, E(x, t), 0)^T, \quad \mathbf{J} = (0, J(x, t), 0)^T$$

so that equations (1,2) reduce to

$$\partial_x B = -\mu_0 J, \quad (5)$$

$$\partial_t B = -\partial_x E. \quad (6)$$

Following [2], the constitutive relation reads

$$E = \rho(J), \quad (7)$$

where ρ is the antisymmetric function defined by

$$\rho(J) = 0.5\rho_0 \left[1 + \tanh\left(\frac{J - J_c}{w}\right) \right] (J - J_c), \quad J > 0 \quad (8)$$

$$\rho(J) = 0.5\rho_0 \left[1 + \tanh\left(\frac{J + J_c}{w}\right) \right] (J + J_c), \quad J < 0. \quad (9)$$

where ρ_0 is the normal resistivity and J_c the critical current density. This form of $\rho(J)$ is a regularized version of the one used by Romero-Salazar et al [2], it is plotted in

Fig. 10. It is close to a standard constitutive law derived from the Bean critical state model [10], see also [9] for a detailed justification. For small J , $E = 0$ so that there is no heating EJ . Only for $J > J_c$, do we have $E > 0$ and the heating term EJ becomes significant.

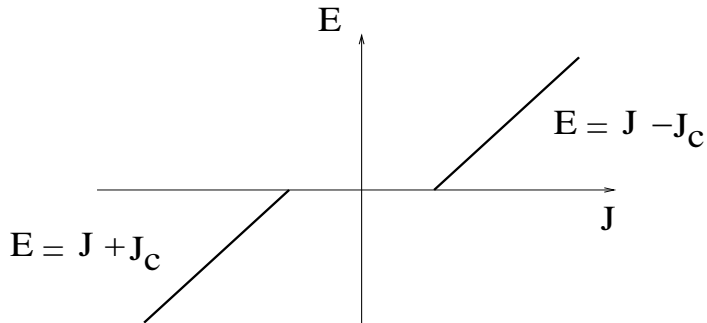


FIG. 2: Plot of $E = \rho(J)$ given by (7,8,9) for small w_j

In the following, we will only describe the situation $J > 0$ and $B > 0$ for simplicity.

For the critical current density J_c , we assume the following standard dependence on T and B

$$J_c = J_0 \left(1 - \frac{T}{T_c}\right) \left(1 - \frac{|B|}{B_c}\right)^2 \quad T < T_c, |B| < B_c, \quad (10)$$

$$J_c = 0, \text{ otherwise}$$

where T_c is the critical temperature, B_c is a threshold magnetic field, and J_0 a typical current density. Contour plots of J_c are presented in Fig. 3 in the plane (T, B) . Note how J_c varies strongly as a function of B .

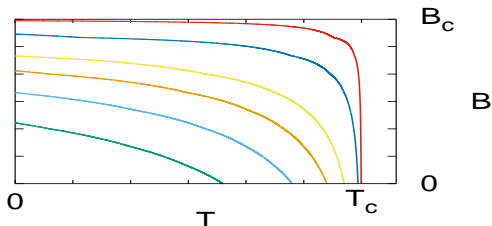


FIG. 3: Plot of J_c given by (10) for the contour lines 0.4, 0.2, 0.1, 0.05, 0.01 and 0.001 from left to right.

Collecting equations (5,6,7) and the temperature equa-

tion, we obtain the system of equations

$$\partial_t B = -\partial_x \left(\rho \left(-\frac{\partial_x B}{\mu_0} \right) \right) \quad (11)$$

$$\rho_m C \partial_t T = -\frac{\partial_x B}{\mu_0} \rho \left(-\frac{\partial_x B}{\mu_0} \right) + \kappa \partial_{xx}^2 T. \quad (12)$$

on the domain $[0, d]$ together with boundary conditions

$$B(x=d) = B_e, \quad T(x=d) = T_e, \quad \text{symmetry at } x=0. \quad (13)$$

like in [2].

To gain intuition, assume a simple ohmic behavior $E = \rho_0 J$. Then the two equations above reduce to diffusion equations and we do not expect any singular behavior. On the other hand, the nonlinearity of the two equations (36, 12) gives rise to interesting effects.

B. Time scales

Table I summarizes the physical quantities used in the model and their dimensions, where M, L, T, I and Θ denote the dimensions of mass, length, time, electric current and temperature respectively. In the model, three

Symbols	Name	Dimension	value in SI unit
B	Magnetic field	$MT^{-2}I^{-1}$	T
E	Electric field	$MLT^{-3}I^{-1}$	Vm^{-1}
J, J_c, J_0, w_j	Current density	$L^{-2}I$	Am^{-2}
T	Temperature	Θ	K
x, d	Position, width	L	m
t	Time	T	s
C	Heat capacity	$L^2\Theta^{-1}$	$m^2 s^2 K^{-1}$
ρ_m	Mass density	ML^{-3}	$kg m^{-3}$
κ	Thermal conductivity	$MLT^{-3}\Theta^{-1}$	$W m^{-1} K^{-1}$
ρ_0	Resistivity	$ML^3T^{-3}I^{-2}$	Ωm
μ_0	Vacuum permeability	$MLT^{-2}I^{-2}$	$kgms^{-2}A^{-2}$

TABLE I: Quantities used in the model, their dimension and unit in the S.I. system.

physical phenomena are coupled: the magnetostatic effects described by (36), the thermal heating due to the electric field given by the first term of the right-hand side of (12) and the thermal diffusion described by the second term of the right-hand side of (12). We can therefore

define three characteristic times:

$$\text{the magnetic timescale: } t_{\text{mag}} = \frac{\mu_0 d^2}{\rho_0}, \quad (14)$$

$$\text{the thermal diffusion timescale: } t_{\text{diff}} = \frac{\rho_m C d^2}{\kappa}, \quad (15)$$

$$\text{the Joule heating timescale: } t_{\text{heat}} = \frac{\rho_m C T}{E J}. \quad (16)$$

To estimate the relative importance of these different time scales, following [2], we consider a plate of thickness d and evaluate the Joule heating term as $EJ \simeq \rho_0 J_c^2$. The values of d , J_c and $C = \rho_m C$ are taken from [2, Table 1]. They are recalled in Table II. The resistivity ρ_0 corre-

Quantity	value in SI unit
d	1 cm
ρ_0	$10^{-8} \Omega\text{m}$
κ	$200 \text{ mW cm}^{-1}\text{K}^{-1}$
$C = \rho_m C$	
ρ_m	2500 kg m^{-3}
C	$50 \text{ m}^2 \text{ s}^2 \text{ K}^{-1}$
B_c	4 T
T_c	39K
J_c	$4 \cdot 10^9 \text{ Am}^{-2}$

TABLE II: Parameter values extracted from [2], [5] and [12].

sponds to the reciprocal of the normal-state conductivity used in [5] and the thermal conductivity is κ as depicted in [12, Fig. 1] for the lowest temperature ($T = 20\text{K}$).

The heat capacity of a material like MgB2 depends on the temperature as shown in Figure of Zou's article [12]. For $20 < T < 50\text{K}$ this dependence is weak and can be neglected, however when $T \rightarrow 0$ $C \rightarrow 0$ so that for small temperatures, one should write

$$C(T) = C_0 T, \quad C_0 = 0.25 \text{ m}^2 \text{ s}^2, \quad (17)$$

to follow the measurements of [12]. This will change the equations and their normalization.

For large temperatures where C can be assumed constant, the resulting time scales are

$$t_{\text{mag}} \approx 1.25 \cdot 10^{-3} \text{ s}; \quad t_{\text{diff}} \approx 0.62 \text{ s}; \quad t_{\text{heat}} \approx 4.81 \cdot 10^{-4} \text{ s}. \quad (18)$$

We therefore conclude that the two dominating effects are the magnetic diffusion and the Joule heating, as they occur on a much shorter timescale than the thermal diffusion.

C. Normalization

We can now proceed with the normalization of the equations. Starting from

$$\partial_x B = -\mu_0 J, \quad (19)$$

$$\partial_t B = -\partial_x E, \quad (20)$$

$$E = \rho(J), \quad (21)$$

$$\rho_m C \partial_t T = \kappa \partial_{xx}^2 T + EJ, \quad (22)$$

we introduce

$$x = dx'; \quad t = t_0 t'; \quad T = T_c T'; \quad B = B_c B' \\ E = E_0 E', \quad J = J_0 J',$$

where E_0 and J_0 will be chosen later and

$$t_0 = t_{\text{heat}} = \frac{\rho_m C T_c}{E_0 J_0}, \quad (23)$$

is a typical Joule heating time t_{heat} . The nonlinear resistivity can be written as

$$\rho(J) = \rho_0 J_0 \rho'(J'), \quad (24)$$

where ρ_0 is the normal state resistivity and

$$\rho'(J') = 0.5 \left[1 + \tanh \left(\frac{J' - J'_c}{w'} \right) \right] (J' - J'_c), \quad (25)$$

$$J'_c = (1 - T')(1 - |B'|)^2, \quad (26)$$

1. High temperature: C constant

Plugging the rescalings above into equations (19), we obtain

$$\frac{B_c}{d} \partial_{x'} B' = -\mu_0 J_0 J', \quad (27)$$

$$\frac{B_c}{t_0} \partial_{t'} B' = -\frac{E_0}{d} \partial_{x'} E', \quad (28)$$

$$E_0 = \rho_0 J_0, \quad (29)$$

$$E' = \rho'(J'), \quad (30)$$

$$\frac{\rho_m C T_c}{t_0} \partial_{t'} T' = \frac{\kappa T_c}{d^2} \partial_{x'x'}^2 T' + E_0 J_0 E' J'. \quad (31)$$

It is therefore natural to take the following value for J_0

$$J_0 = \frac{B_c}{\mu_0 d}. \quad (32)$$

We also define

$$E_0 = \rho_0 J_0, \quad (33)$$

to obtain

$$E = \rho(J), \quad (34)$$

$$\partial_x B = -J, \quad (35)$$

$$\partial_t B = -\alpha \partial_x E, \quad (36)$$

$$\partial_t T = EJ + \beta \partial_{xx}^2 T, \quad (37)$$

where the primes have been dropped for clarity and the parameters α, β are given by

$$\alpha = \frac{t_0}{t_{\text{mag}}} = \frac{\rho_m C T_c \mu_0}{B_c^2}; \quad \beta = \frac{t_0}{t_{\text{diff}}} = \frac{\kappa T_c \mu_0^2}{\rho_0 B_c^2}. \quad (38)$$

With the values of the parameters, we find

$$\alpha \approx 0.38; \quad \beta \approx 7.69 \cdot 10^{-4}. \quad (39)$$

The system of equations (35,36,34,37) can be written in a compact form by eliminating E and J . We get

$$B_t = \alpha \partial_x [\rho(B_x)], \quad (40)$$

$$T_t = B_x \rho(B_x) + \beta T_{xx}, \quad (41)$$

where the partial derivatives are written as indices to simplify notation. Note that the minus sign in equations (35,36) is absent since ρ is antisymmetric.

2. Low temperature: $C(T)$

When $C(T) = C_0 T$, the equations become

$$B_t = \alpha \partial_x [\rho(B_x)], \quad (42)$$

$$TT_t = B_x \rho(B_x) + \beta T_{xx}, \quad (43)$$

where the coefficients α, β are given by

$$\alpha = \frac{t_0}{t_{\text{mag}}} = \frac{\rho_m C_0 T_c^2 \mu_0}{B_c^2}; \quad \beta = \frac{t_0}{t_{\text{diff}}} = \frac{\kappa T_c \mu_0^2}{\rho_0 B_c^2}. \quad (44)$$

With the values of the parameters, we find

$$\alpha \approx 7.5 \cdot 10^{-2}; \quad \beta \approx 7.69 \cdot 10^{-4}. \quad (45)$$

The time scales are now

$$t_{\text{mag}} \approx 1.25 \cdot 10^{-3} \text{ s}; \quad t_{\text{diff}} \approx 0.12 \text{ s}; \quad t_{\text{heat}} \approx 9.38 \cdot 10^{-5} \text{ s}. \quad (46)$$

3. Boundary conditions

From (13) the normalized boundary conditions for both (40,41) and (42,43) are

$$B(x=1) = B_e, \quad T(x=1) = T_e, \quad \text{symmetry at } x=0. \quad (47)$$

The systems of equations (40,41) and (42,43) together with the boundary conditions (47) are our main equations and will be analyzed in the next sections.

III. NUMERICAL METHOD

The system of equations (35,36,34,37) was discretized in space using second order finite differences and the time advance was done using an ordinary differential equation solver, typically a Runge-Kutta method.

For the spatial discretization, we introduce an N -points grid for the spatial domain $[0, 1]$

$$0 = x_0 < x_1 < \dots < x_{N-1} = 1, \quad (48)$$

where

$$x_j = j \Delta x, \quad \text{and} \quad \Delta x = \frac{1}{N-1}. \quad (49)$$

Let B_j^n, T_j^n, E_j^n and J_j^n be the approximations of B, T, E and J at time $t_n = n \Delta t$ and at point x_j respectively. For constant C , assuming a simple Euler time discretization, equations (35,36,34,37) yield

$$J_j^n = \frac{B_{j+1}^n - B_{j-1}^n}{2 \Delta x}, \quad (50)$$

$$E_j^n = \rho(J_j^n, T_j^n), \quad (51)$$

$$\frac{B_j^{n+1} - B_j^n}{\Delta t} = \alpha \frac{E_{j+1}^n - E_{j-1}^n}{2 \Delta x}, \quad (52)$$

$$\frac{T_j^{n+1} - T_j^n}{\Delta t} = E_j^n J_j^n + \beta \frac{T_{j+1}^n - 2T_j^n + T_{j-1}^n}{\Delta x^2}, \quad (53)$$

for interior grid points. For variable C , the last equation reads

$$T_j^n \left(\frac{T_j^{n+1} - T_j^n}{\Delta t} \right) = E_j^n J_j^n + \beta \frac{T_{j+1}^n - 2T_j^n + T_{j-1}^n}{\Delta x^2}.$$

We used off-centered differences to handle the two boundary points $x = 0, 1$. The time advance from B_j^n, T_j^n to B_j^{n+1}, T_j^{n+1} uses the following algorithm

- (i) Compute J_j^n using (50),
- (ii) Compute E_j^n using (51),
- (iii) Compute B_j^{n+1}, T_j^{n+1} using (52,53).

To ensure the stability of the method, N or Δt are chosen such that the Courant-Friedrich-Levy stability condition [11]

$$\alpha \frac{\Delta t}{\Delta x^2} < 1, \quad (54)$$

holds. To gain accuracy, we used an explicit fourth-order Runge-Kutta method for the time integration. In most runs, we used

$$dx = 10^{-2}, \quad dt = 10^{-5},$$

because α is small. Some numerical experiments have also been carried out using a *Total Variation Diminishing* (TVD) Runge-Kutta scheme, leading to similar numerical results.

A. Magnetic field pulse

Before describing in detail the results, we make the following remarks.

- Care must be taken in handling the situations $E < 0$ and $J < 0$.
- We observe numerically that calculations cannot be started with B_e large because of instabilities.
- Because of the symmetry condition, $B(x)$ is not differentiable at $x = 0$. We therefore enforce $J(0) = \partial_x(B)(0) = 0$ to stabilize the numerical method. Otherwise, we observe an instability of the scheme.
- The critical current J_c is temperature dependent and it is zero for $T > T_c$.

We use a magnetic field $B_e(t)$ that ramps up from 0 to B_{max} and back to 0, see Fig. 4.

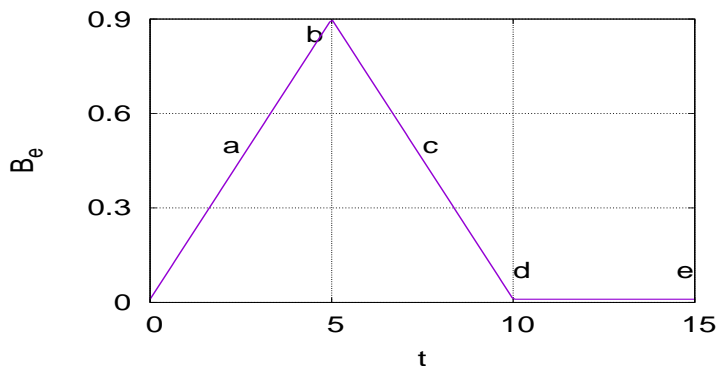


FIG. 4: Plot of $B_e(t)$ for a magnetic field pulse with $B_{max} = 0.9$.

We denote by t_p the duration of the magnetic pulse $B_e(t)$, in Fig. 4 $t_p = 10$.

IV. NUMERICAL RESULTS FOR CONSTANT C

We first consider a medium temperature $T < 1 (= T_c)$ for which we can assume the heat capacity to be constant. Then we use equations (40,41) and parameters α, β given by (39).

A. Influence of B_e for $T_e = 0.5$

Fig. 5 shows snapshots of $B(x), T(x), E(x)$ and $J(x)$ from top left to bottom right for the five time instants a, b, c, d and e corresponding to the magnetic pulse of Fig. 4. Note how B increases gradually. The evolution of B_t

is given by

$$B_t = \alpha \rho_{B_x} [2(1-T)(1-B)B_x + B_{xx} + 2(1-B)^2 T_x], \quad (55)$$

see the Appendix for the derivation. This shows that as long as ρ_{B_x} remains zero B i.e. for $B_x < J_c$, then B does not change. When $\rho_{B_x} \neq 0$, three terms contribute to the evolution of B : the first term in the bracket is a convection term, the second is a diffusion term. These two terms correspond to a Burger's front type dynamics [13], [14] for the magnetic field entering the sample. The third term is unexpected and gives a global evolution of B . This term is responsible for the flux jumps. We analyze it's effect below.

Neglecting the evolution of T we can compute the fixed point of the equation above and get

$$B(x) = 1 - \frac{1}{(1-B_e)^{-1} - J_c^*(1-T)(1-x)}, \quad (56)$$

where $J_c^* \approx 1$ as shown in the Appendix. This expression is in agreement with the snapshots of Fig. 5.

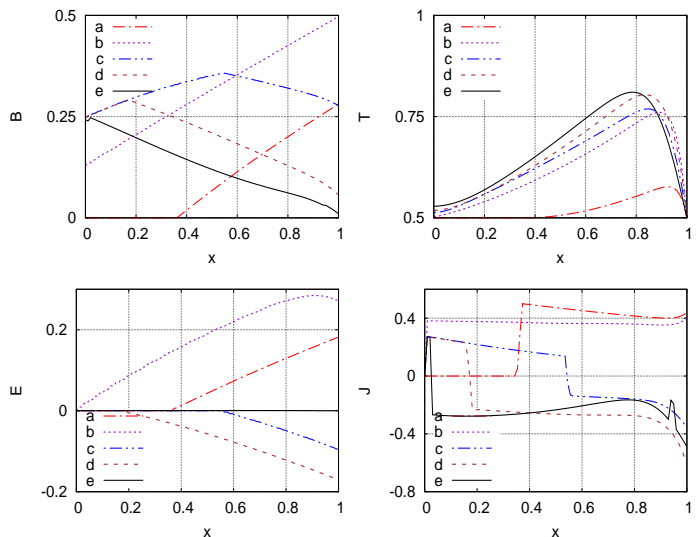


FIG. 5: Plots of $B(x), T(x)$ (top) and $E(x), J(x)$ (bottom) for a field pulse with $B_{max} = 0.5$. The plots correspond respectively to labels a,b,c,d and e in Fig. 4. The external temperature is $T_e = 0.5$.

Notice how for snapshot (b) B is blocked at $x = 0.4$ because $J = 0$ for $x > 0.4$; there is no diffusion. At (c) we have a large temperature increase so that B increases strongly. The temperature does not change significantly after that. For snapshot (e), after the pulse has passed, there is a trapped field B and a non zero current J .

Increasing B_{max} to 0.9, we observe that the sample becomes normal. The snapshots are shown in Fig. 6.

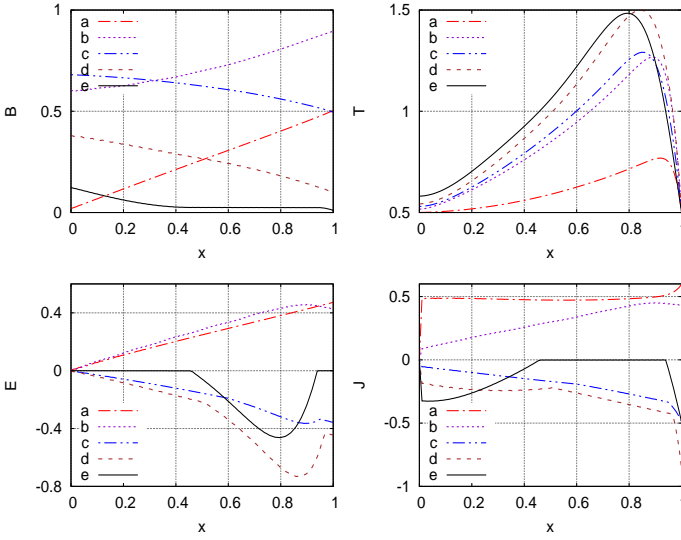


FIG. 6: Same as Fig. 5 except $B_{max} = 0.9$.

Notice the linear profile for (a), in agreement with (18). The temperature develops a gradient so that the last term in (55) becomes significant and causes a large increase in B for snapshot (b). After the pulse has passed, the trapped field is small even though B_{max} was large. Notice the zero regions in E and J where $J_c = 0$.

B. Magnetization

To measure the trapped field induced by a magnetic field pulse, we computed the magnetization in the sample as

$$M = \int_0^1 (B(x) - B_e) dx \quad (57)$$

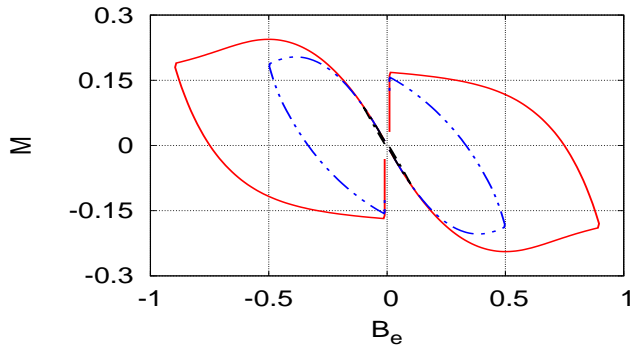


FIG. 7: Plots of $M(B_e)$ for field pulses of duration $t_p = 10$ and $B_{max} = 0.9$ (red online), 0.5 (blue online) and 0.1 (black online). The external temperature is $T_e = 0.5$.

Note that the curve for B_e ramped up to $B_{max} = 0.9$

(red online) drops down to 0 after the pulse has passed. This is because the sample has turned normal so that there is no trapped field. On the contrary for $B_{max} = 0.5$ (blue online), there is a small dip that stops. Here, the sample remains superconductor and there is a trapped field. For $B_{max} = 0.1$ (black online) the trapped field is very small, this shows that nonlinear effects are important to trap a magnetic field. Finally note that the curves are smooth, so that there are no flux jumps for these parameters.

C. Pulse duration

To prevent the sample from turning normal, one can lengthen the duration t_p of the magnetic field pulse. Taking the parameters of Fig. 6 and applying the pulse over a duration $t_p = 100$ instead of 10 prevents the sample from turning normal. The results are presented in Fig. 8. Again we observe a linear profile for snapshot (a) in agreement with (18). The temperature does not change much and B follows B_e . Notice the trapped field after the pulse has passed, it is comparable to the one for $B_{max} = 0.5$ and $t_p = 10$.

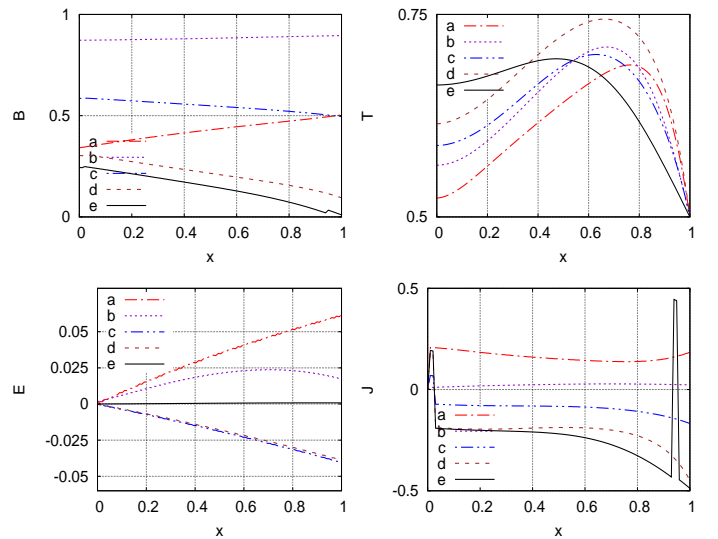


FIG. 8: Same as Fig. 6 except B_e is ramped up over a duration $t_p = 100$.

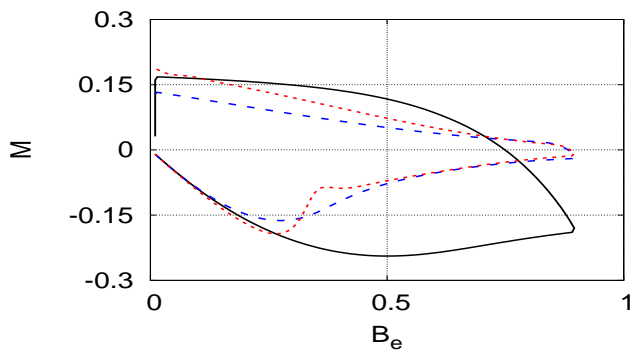


FIG. 9: Magnetization for pulse duration $t_p = 10$ (black on-line) 100 (long dash, blue online) and 1000 (short dash, red online).

The magnetization is shown in Fig. 9 for $t_p = 10$, 100 and 1000. For a duration $t_p = 10$, there is no trapped field as the sample has turned normal. Notice how M decays slowly for the red curve. For a duration of 100, the sample remains superconductor, there is a trapped field. The trapped field is larger for a duration of 1000 since the heating caused by the external field has time to dissipate.

To conclude this section, we consider a long duration $t_p = 1000$ and compare in Fig. 10 the magnetizations for $B_{max} = 0.5$ and 0.9 . Notice the larger trapped field for $B_{max} = 0.5$. For this field we observe a first flux jump for $B_e = 0.3$, we come back to this issue in the next section.

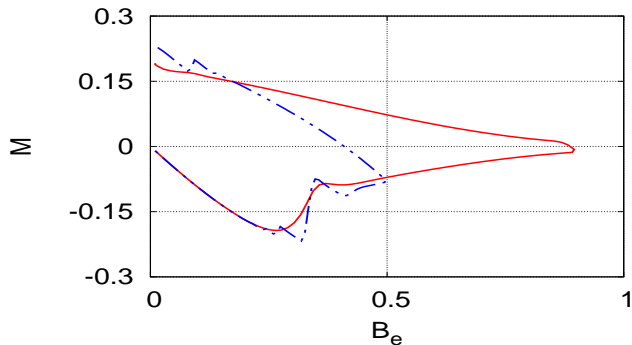


FIG. 10: Magnetization $M(B_e)$ for pulse duration $t_p = 1000$ for a field $B_e(t)$ ramped up to 0.9 (red online) and 0.5 (blue online).

V. NUMERICAL RESULTS FOR $C(T)$

For small temperatures, the dependence $C(T)$ cannot be neglected. We now study solutions of the system of equations (42,43) and parameters α, β given by (45). Throughout this section, we assume a small temperature

$$T_e = 0.1.$$

A. Influence of B_e for $T_e = 0.1$

We first test a small magnetic pulse with $B_{max} = 0.1$. The snapshots are shown in Fig. 11. Notice the large temperature increase from (a) to (b) for a moderate field increase. This is because the temperature equation involves T^2 and not T . For the subsequent snapshots, the temperature does not change much. The field penetrates very little inside the material and the trapped field is small.

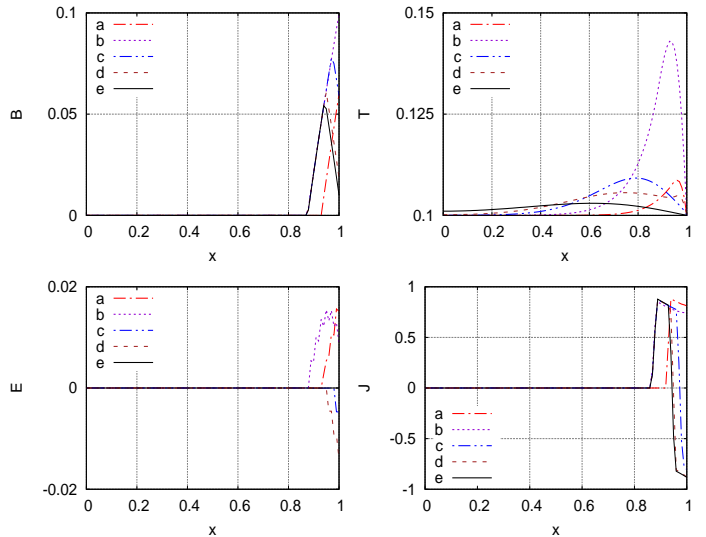


FIG. 11: Plots of $B(x), T(x)$ (top) and $E(x), J(x)$ (bottom) for a field pulse such that $B_{max} = 0.1$. The Labels a,b,c,d and e are indicated in Fig. 4.

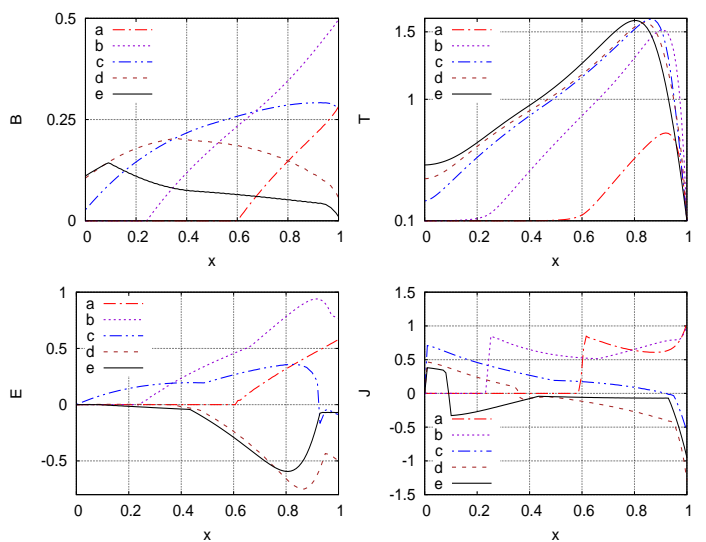


FIG. 12: Same as Fig. 11 except B_e is ramped up to 0.5 and back down.

The effect of a larger pulse $B_{max} = 0.5$ is shown in Fig. 12. Again notice the large temperature increase from (a) to (b), there part of the sample has lost its superconductivity. Then $J_c = 0$ and B is small for snapshot (e) and will continue to decay. Notice how both E and J are not zero for (e) so the term EJ remains significant and drives this decay of B .

Increasing the duration of the pulse to $t_p = 100$ for the last set of parameters does not prevent the sample from turning normal. Again, this is probably due to the temperature equation which evolves T^2 . Only increasing to a duration $t_p = 1000$ does the sample remain superconductor.

B. Flux jump in magnetization : optimal B_e and pulse duration

We observed a small flux jump for a long duration pulse for a constant heat capacity C . Let us examine the situation $C(T)$. Fig. 13 shows the magnetization vs B_e for pulse durations $t_p = 600, 1500, 3000$. Notice that $M(B_e)$ is smooth for $t_p = 600$ and presents large flux jumps for $t_p = 1500$ and 3000 . Notice that they do not occur at the same values of B_e .

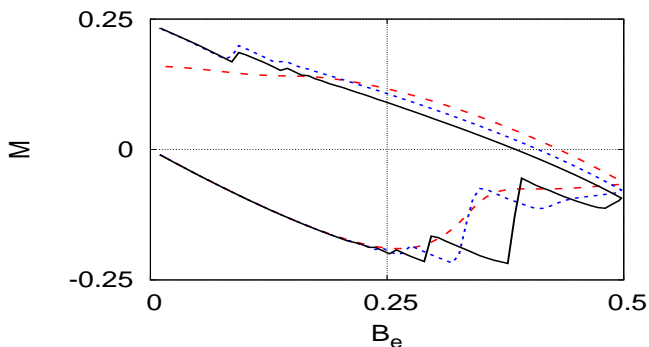


FIG. 13: Magnetization $M(B_e)$ for field pulses with $B_{max} = 0.5$ and pulse durations $t_p = 600$ (long dash, red online), 1500 (short dash, blue online) and 3000 (continuous, black online). The temperature is $T_e = 0.1$.

To understand the mechanism of these flux jumps, we consider in detail the pulse duration $t_p = 3000$. The flux jumps occur for $B_e = 0.3$ and 0.37 as B_e is increasing. The snapshots are shown in Fig. 14. As expected there is a large increase of temperature from (a) to (b). The field B also exhibits a large increase. Notice how EJ is negative for snapshots (b) and (d).

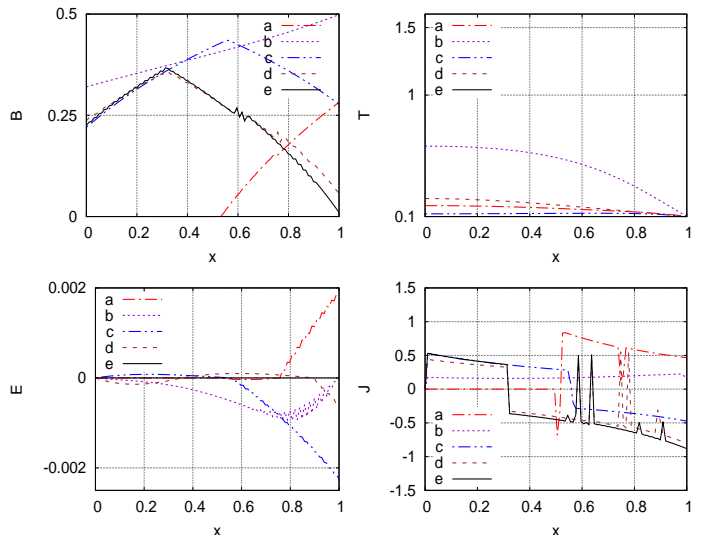


FIG. 14: Plots of $B(x), T(x)$ (top) and $E(x), J(x)$ (bottom) for a field pulse with $B_{max} = 0.5$ and $t_p = 3000$. The external temperature is $T_e = 0.1$.

We now present a detailed analysis of the two flux jumps observed for $B_e = 0.3$ and $B_e = 0.37$. The fields $B(x), T(x), E(x), J(x)$ and $J_c(x)$ are shown in Fig. 15 for times $t = 570, 585$ and 600 . The time step is $dt = 10^{-4}$ in units of t_{heat} . Note how the temperature increases strongly from $t = 570$ to $t = 585$. The third term in equation (58) becomes large and causes a large increase in B observed for $t = 585$. Notice how B does not vary much after the flux jump from $t = 585$ to 600 . The oscillations of E are due to $J \approx J_c$. The spikes observed in J correspond to jumps in B_x , these are due to the irregular Burger's front dynamics of B .

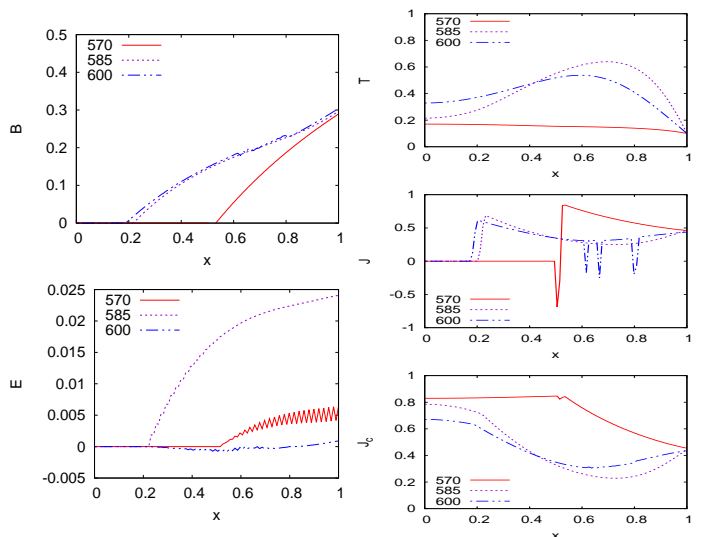


FIG. 15: Plots of $B(x), T(x)$ (top) and $E(x), J(x), J_c(x)$ (bottom) for three successive times $t = 570, 585$ and 600 .

The dynamics of the other large flux jump observed for $B_e = 0.37$ is shown in Fig. 16. Notice the large increase in T from $t = 750$ to 765 so that B has increased. The temperature continues to evolve at $t = 780$ so that B increases again. At time $t = 795$, B has settled down, there is little difference between $B(780)$ and $B(795)$. The temperature continues to evolve however because of the $B_x \rho(B_x)$ term.

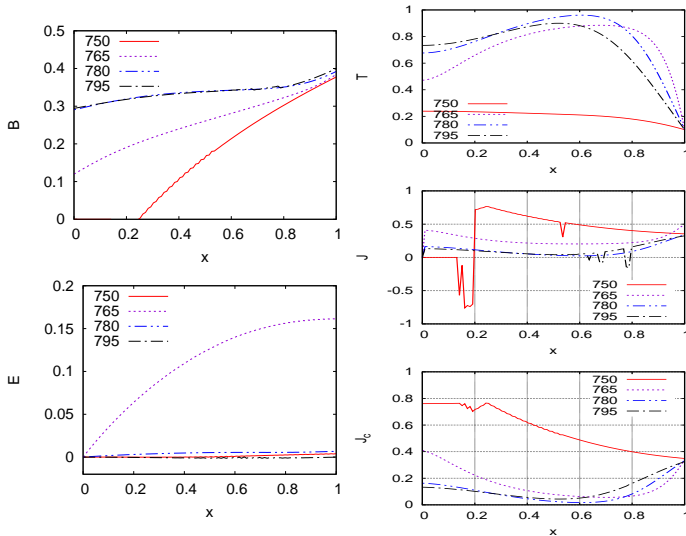


FIG. 16: Plots of $B(x), T(x)$ (top) and $E(x), J(x), J_c(x)$ (bottom) for three successive times $t = 750, 765, 780$ and 795 .

VI. CONCLUSION

We analyzed mathematically and numerically a flux-jump model for type II superconductors in a 1D configuration where the magnetic field is a scalar B . The model involves a nonlinear diffusion equation for B coupled to a diffusion equation for the temperature T . In addition the critical current J_c depends on the magnetic field B and the temperature T .

We determined the typical time scales of the Joule heating, magnetic field dynamics and temperature diffusion for MgB_2 and YBaCuO from the literature. Non dimensionalizing the equations using the Joule heating time, we could understand better the mathematical couplings between the different fields. We considered how the system responds to an incoming magnetic field pulse.

The dynamics of B is given by an inhomogeneous Burger's convection-diffusion equation whose solutions are fronts. These fronts have an irregular speed because of the inhomogeneities. In addition, there is a global nonlinear driving term $(1 - B)^2 T_x$ and this is responsible for the flux jumps. We observed that flux jumps occur mostly at low temperature and medium magnetic fields, which is consistent with the global driving term. Flux jumps are always preceded by large increases in T and T_x .

Regarding the question of the optimization of trapped fields, we varied the incoming pulse duration in different conditions. For medium temperatures, we found that large pulse durations maximize the trapped field and can cause flux jumps. If the incoming pulse is too large, the sample turns normal and any trapped field quickly dissipates with time. At low temperatures, the heat capacity is no longer constant so that the T equation becomes nonlinear. Here, again for large duration pulses, we observe larger flux jumps and slightly larger trapped fields.

A future study could be to examine different forms of the incoming magnetic field $B_e(t)$ to see if we can increase the trapped field and reduce flux jumps. In a more realistic setting, one could look for an adapted sample geometry to maximize this trapped field.

Acknowledgements: The authors thank J. Durrell for useful discussions. N. R. acknowledges the support of the Normandie Regional Government and the European Union through grant "Supramag". The authors thank the Centre Régional Informatique et d'Applications Numériques de Normandie for using its computational resources.

-
- [1] J. H. Durrell, M. D. Ainslie, D. Zhou, P. Vanderbemden, T. Bradshaw, S. Speller, M. Filipenko and D. A. Cardwell, Bulk superconductors: a roadmap to applications, *Supercond. Sci. Technol.* 31 (2018) 103501
 - [2] C. Romero-Salazar, F. Morales, R. Escudero, A. Durán, O. A. Hernández-Flores, Flux jumps in hot-isostatic-pressed bulk MgB_2 superconductors: Experiment and theory *Physical Review B* 76, 104521,(2007).
 - [3] M. D. Ainslie, D. Zhou, H. Fujishiro, K. Takahashi, Y.-H. Shi and J. H. Durrell, Flux jump-assisted pulsed field magnetisation of high- J_c bulk high-temperature superconductors, *Supercond. Sci. Technol.* 29 (2016) 124004
 - [4] J.-G. Caputo, I. Danaïla and C. Tain, An Abelian Higgs model of pulsed field magnetisation in superconductors, *J. Physics : Conference Series*, 2043, 012006, (2021).
 - [5] M. Fracasso et al, Numerical study on flux-jump occurrence in a cup-shaped MgB_2 bulk for magnetic shielding applications *Supercond. Sci. Technol.* 36 (2023) 044001
 - [6] A.M. Campbell and J.E. Evetts (1972) Flux vortices and transport currents in type II superconductors, *Advances in Physics*, 21:90, 199-428, DOI: 10.1080/00018737200101288
 - [7] D. R. Heron D. R. and S. J. Chapman, A Hierarchy of Models for Superconducting Thin Films, *SIAM Journal on Applied Mathematics*, 63, 2087-2127, (2003).
 - [8] V. Ciantanni and M. D. Ainslie, Modelling and mitigating flux jumps in bulk high-temperature superconductors during quasi-static, high-field magnetisation, *Supercond.*

Sci. Technol. 36 (2023) 025007

- [9] C. J. van Der Beek and P. H. Kes, Flux pinning, Handbook of Superconductivity: Fundamentals and Materials, Volume One (2nd ed.). Cardwell, D.A., Larbalestier, D.C., and Braginski, A. (Eds.). (2021). CRC Press. <https://doi.org/10.1201/9780429179181>
- [10] P. S. Swartz and C. P. Bean, J. Appl. Phys. 39, 4991–8, (1968).
- [11] W. Strauss, Partial differential equations: an introduction, Wiley (2007).
- [12] J Zou et al, Supercond. Sci. Technol. 28 075009, (2015).
- [13] G. B. Whitham, Linear and nonlinear waves, Wiley, (1974).
- [14] J.-G. Caputo et Y. Stepanyants, "Front solutions of Richards equation", "Transport in porous media", 74, 1-20, (2008).

VII. APPENDIX: FIXED POINT OF THE EQUATIONS AND OSCILLATIONS OF B

If the heat capacity is large and the pulse is short, one can neglect the evolution of the temperature and assume $T(x) = T_e$. Then equations (40,41) decouple and we can look for a fixed point of equation (40). This is the object of this section.

Denoting the partial derivatives as subscripts for simplicity of writing, we have

$$\begin{aligned} B_t &= \alpha \partial_x [\rho(B, B_x, T)], \\ &= \alpha (\rho_B B_x + \rho_{B_x} B_{xx} + \rho_T T_x). \end{aligned}$$

From

$$\rho(B_x) = 0.5 \left[1 + \tanh\left(\frac{B_x - J_c}{w}\right) \right] (B_x - J_c),$$

and

$$J_c = (1 - T)(1 - B)^2,$$

we can calculate the different terms $\rho_B, \rho_{B_x}, \rho_{J_c}, \rho_T$ and obtain

$$\begin{aligned} \rho_{B_x} &= \frac{0.5}{w} \left[1 - \tanh^2\left(\frac{B_x - J_c}{w}\right) \right] (B_x - J_c), \\ &\quad + 0.5 \left[1 + \tanh\left(\frac{B_x - J_c}{w}\right) \right], \\ \rho_{J_c} &= -\rho_{B_x}, \\ \rho_B &= \rho_{J_c} J_{cB} = \rho_{B_x} 2(1 - T)(1 - B), \\ \rho_T &= \rho_{J_c} J_{cT} = \rho_{B_x} 2(1 - B)^2. \end{aligned}$$

Then the evolution of B is given by

$$B_t = \alpha \rho_{B_x} [2(1 - T)(1 - B)B_x + B_{xx} + 2(1 - B)^2 T_x]. \quad (58)$$

Since ρ_B and ρ_T are proportional to ρ_{B_x} , the fixed point $B_t = 0$ corresponds to $\rho_{B_x} = 0$.

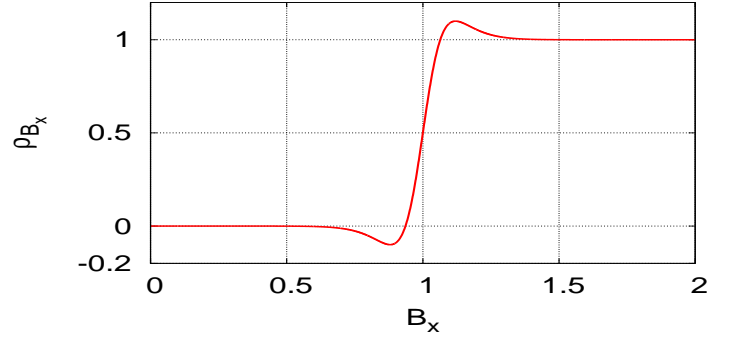


FIG. 17: Plot of ρ_{B_x} as a function of B_x for $J_c = 1$ and $w = 0.1$.

The evolution of ρ_{B_x} is shown in Fig. 17, the function crosses 0 for

$$B_x = J_c^* \approx 1 - w.$$

For example, for $w = 0.1$, we get $J_c^* = 0.93$.

Then, to obtain the fixed point, we need to solve the equation

$$B_x = 0.93(1 - T)(1 - B)^2 \quad (59)$$

together with the boundary conditions (47). From (59) we get

$$\frac{B_x}{(1 - B)^2} = 0.93(1 - T),$$

Assuming, $T = T_e$ this is a separable differential equation which can be integrated as

$$\int_B^{B_e} \frac{dB}{(1 - B)^2} = \int_x^1 0.93(1 - T_e) dx,$$

to yield the final result

$$B(x) = 1 - \frac{1}{(1 - B_e)^{-1} - 0.93(1 - T)(1 - x)}. \quad (60)$$

Fig. 18 shows this expression as a blue line together with the numerical solution in red for $B_e = 0.18, 0.51$ and 0.844 in Fig. 18 for $T_e = 0.3$. The other parameters are $\alpha = 10, \beta = 7.69 \cdot 10^{-4}$.

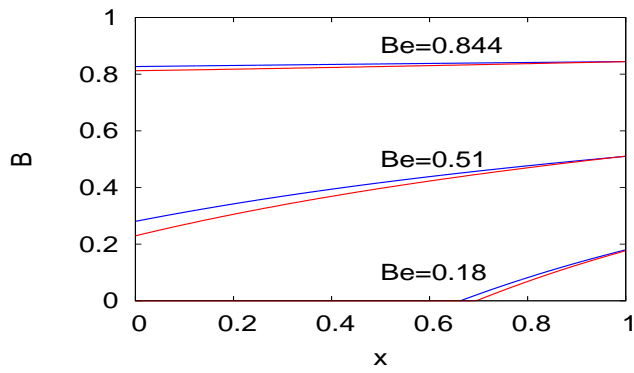


FIG. 18: Plots of $B(x)$ for $B_e = 0.18, 0.51$ and 0.844 , the approximation is shown in blue while the numerical solution is in red.

The dominating term is $\rho_{B_x} B_{xx}$ because $(1 - T)(1 - B) < 1$ and $(1 - B)^2 < 1$. This is a diffusion with oscillating diffusion coefficient.